

# Excitation-induced effects in selenium clusters: molecular-orbital analyses

K. TANAKA

*Department of Applied Physics, Graduate School of Engineering, Hokkaido University, Sapporo, Japan*

Covalent chalcogenide glasses are known to exhibit unique features, including p-like conduction, midgap photoluminescence and photoinduced phenomena. To obtain fundamental insights into such characteristics, addition effects of an electron, hole and exciton to an  $\text{Se}_8$  ring and  $\text{H-}n\text{Se-H}$  ( $n \leq 10$ ) chains have been analyzed using an *ab initio* molecular-orbital calculation package GAMESS. The electron addition tends to expand or dismember the clusters, the hole compacts them, and the exciton produces distortions. In chain dimers, a hole enhances interchain interaction through  $\pi$ -type wavefunctions. These deformations accompany polaronic energy shifts, which are consistent with higher hole mobility and sub-midgap luminescence in amorphous and trigonal Se. When the deformed clusters are neutralized or deexcited, successive relaxation recovers initial structures, with a few exceptions that produce disordered clusters and intimate valence-alternation pairs, which may cause meta-stable photoinduced structural changes.

(Received May 22, 2017; accepted October 10, 2017)

*Keywords:* Selenium, Polaron, electronic properties, Photoinduced phenomena

## 1. Introduction

It has been known from the last century that the covalent chalcogenide glass possesses some unique characters [1-3]. For instance, almost of all the chalcogenide glasses exhibit *p-like* conduction [4], i.e. the electrical conductivity being governed by hole motion (not by the density as in the p-type conduction). It has also been demonstrated that photoluminescence appears around photon energies corresponding approximately to half-gaps, while in amorphous (a-) Se the peak is located lower than the half-gap energy [3, 5]. In addition, the chalcogenide glass undergoes structural transformations upon electronic excitations by light, x-ray,  $\gamma$ -ray, and charged particles [1-3]. The transformations are of various kinds, including photo-crystallization, darkening, and deformation, the behaviors varying widely with temperatures, radiation energies, light polarizations, etc. Besides, in a-Se, photoconduction is likely to generate harmful defects [4]. It has also been known that some photoinduced changes appear in isolated Se clusters in vacuum [6, 7] and in zeolite pores [8-10]. Nevertheless, despite of extensive studies, underlying mechanisms of these characteristics remain speculative and/or controversial.

For such long-standing problems, computer analyses have put forward valuable insights. In detail, the analyses include two kinds of approaches, molecular dynamics (MD) [2, 11-14] and chemical calculations such as molecular-orbital (MO) methods [15-20], which have provided inspiring, somewhat complementary results; the former tracing temporal variations within limited durations ( $\leq 5$  ps [14]) and the latter dealing with stationary properties

of modeled structures. And, these calculations follow so-called empirical or *ab initio* procedures. We then expect that further explorations using such numerical analyses will add new perspectives on elemental processes of the electronic properties.

In the present work, we focus on a prototypical material Se, which is characteristic in two respects [1-3]. One is the bonding structure; it is a monatomic system, and in the trigonal phase and also in amorphous structures the homopolar bond -Se-Se- forms polymeric chains, similarly to those in many organic materials such as polyethylene -(CH<sub>2</sub>)-. The other is that it can be regarded as the simplest lone-pair (LP) semiconductor, in which the valence and the conduction band have different origins, being composed of  $\pi^*$ -type LP and anti-bonding ( $\sigma^*$ ) states, respectively.

To understand more deeply the material, we explore fundamental excitation effects through calculating structural and electronic changes in an  $\text{Se}_8$  ring,  $\text{H-}n\text{Se-H}$  chains ( $n \leq 10$ ), and a  $\text{H-2Se-H}$  dimer upon addition of an electron, hole, and exciton. The results will simulate photoinduced changes in isolated Se clusters [6-10]. In addition, provided that a-Se is composed mainly with entangled chains consisting of segments with  $\sim 5$  atoms [21-23], each segment may behave most independently as a fragment, so that the cluster calculation will provide basic insights into the electronic properties and radiation effects in a-Se.

## 2. Calculations

The present analysis utilized an *ab initio* MO calculation package GAMESS [24] operating on a visualization platform Winmostar [25]. A selected base function was of the 6-31+G\* type and the B3LYP-DFT approximation was adopted, the combination having been demonstrated to provide satisfactory results with acceptable computation times [26, 27].

Calculations proceeded in general as follows: At the outset, a neutral Se cluster was produced through optimizing the total (electronic plus structural) energy  $E_T$  under the RHF approximation, the result corresponding to the equilibrium ground state,  $G(q_0)$  in Fig. 1. Addition of an electron (or a hole) was modeled by charging the cluster to  $-e$  ( $+e$ ) under the UHF approximation with the  $q_0$  configuration. On the other hand, addition effects of an electron-hole pair (singlet exciton) were analyzed using the RHF-excite mode under the time-dependent DFT approximation, which provides the smallest electronic excitation energy with a combination of all wavefunctions. (Triplet-exciton states could not be evaluated by GAMESS.) These calculations gave the excited state,  $E(q_0)$  in the figure. The charged or excited cluster was then energy-optimized to a lattice-deformed polaronic state  $E(q)$ . The total energy difference  $\Delta E_T = E_T(E(q_0)) - E_T(E(q))$  in the excited state gives the polaron energy  $E_p$ . Then, the charge or excitation was taken away (the cluster being neutralized), giving rise to a temporal state  $G(q)$ . Finally, the cluster was energy-optimized again, in order to examine whether the structure  $q$  relaxes to the initial configuration  $q_0$  or to an alternative  $q'$ , the processes being referred to as *transitory* and *memorable*.

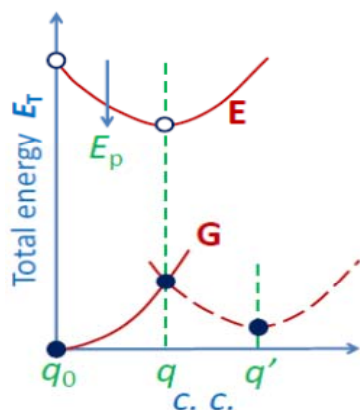


Fig. 1. Total energy  $E_T$  as a function of a configuration coordinate *c.c.*.  $G$  and  $E$  denote the ground and the excited state, and  $q_0$ ,  $q$ , and  $q'$  are, respectively, the initial, polaronic, and meta-stable configurations. The transitory and the memorable change proceed as  $G(q_0) \rightarrow E(q_0) \rightarrow E(q) \rightarrow G(q) \rightarrow G(q_0)$  and  $G(q_0) \rightarrow E(q_0) \rightarrow E(q) \rightarrow G(q) \rightarrow G(q')$ . For the cases of electron addition, the  $E$  curve shifts down-wardly by an amount comparable to the HOMO-LUMO gap.

We here add three remarks: First, high-energy radiation and photoconduction tend to generate free electrons and holes, which will cause the charging effects. Second, bandgap illumination excites electron-hole pairs, which may behave as molecular excitons. Finally, upon excitonic excitation with photon energy of  $E_{PLE} = E_T(E(q_0)) - E_T(G(q_0))$ , luminescence may appear at  $E_{PL} = E_T(E(q)) - E_T(G(q))$ .

## 3. Results and discussion

### 3.1. Se<sub>8</sub> ring

Fig. 2(a, a') shows the energy-optimized ( $G(q_0)$ ) Se<sub>8</sub> ring with the HOMO and LUMO wavefunctions. The ring has a circular crown-shaped structure, characterized by the bond length  $r = 2.37$  Å, bond angle  $\theta = 108^\circ$ , dihedral angle  $\varphi = 99^\circ$ , and ring diameter  $D = 5.43$  Å, which are comparable with experimental results;  $r = 2.32$  Å,  $\theta = 106^\circ$ ,  $\varphi = 101^\circ$ , and  $D = 5.24$  Å [28]. The HOMO-LUMO energy gap  $E_{HL}$  is 3.83 eV and the total energy  $E_T$  is  $-19209.451$  H, which is taken as a reference  $\pm 0$  eV in the following.

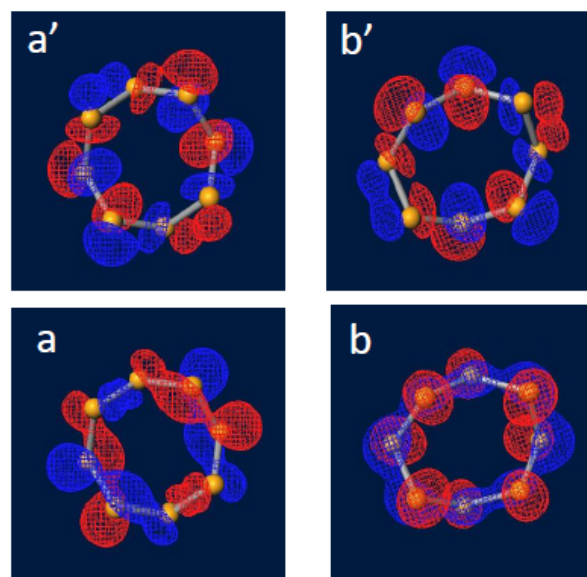


Fig. 2. Top views of Se<sub>8</sub> ring with the HOMO (lower) and LUMO (upper) wavefunctions in (a, a') the initial  $G(q_0)$  and (b, b') the electron-induced  $G(q)$ .

Fig. 3 traces electron-addition effects. The electron enters into the LUMO level (Fig. 2(a')), which was originally located at  $-3.06$  eV, as shown in the figure. The addition makes the level half-filled and its energy rises to  $-0.21$  eV. Concomitantly, the total energy *decreases* (stabilizes) by  $-1.6$  eV. That is, the  $E$  curve in Fig. 1 is located below  $G$  in this case, which is ascribable to enhanced polarization effects. Then, the ring deforms with  $E_p (= E_T(E(q_0)) - E_T(E(q))) = 0.41$  eV to  $E(q)$  (Fig. 2(b, b')), which has an ellipsoidal shape with  $D = 5.20$  and  $6.07$  Å.

The deformation also accompanies  $r$  lengthening to  $\sim 2.42$  Å,  $\theta$  widening to  $\sim 112^\circ$ , and  $\varphi$  scattering to  $82 - 107^\circ$ . Such a deformation is attributable to strong Coulombic repulsion arising from the  $\sigma^*$  state localized on Se-Se bonds. Next, when the electron is deleted,  $G(q)$ ,  $E_{\text{HL}}$  shrinks to 2.74 eV with the HOMO and LUMO wavefunctions shown in Fig. 2(b, b'). Finally, successive relaxation recovers the original structure  $q_0$ , demonstrating that the induced structure  $q$  is transitory.

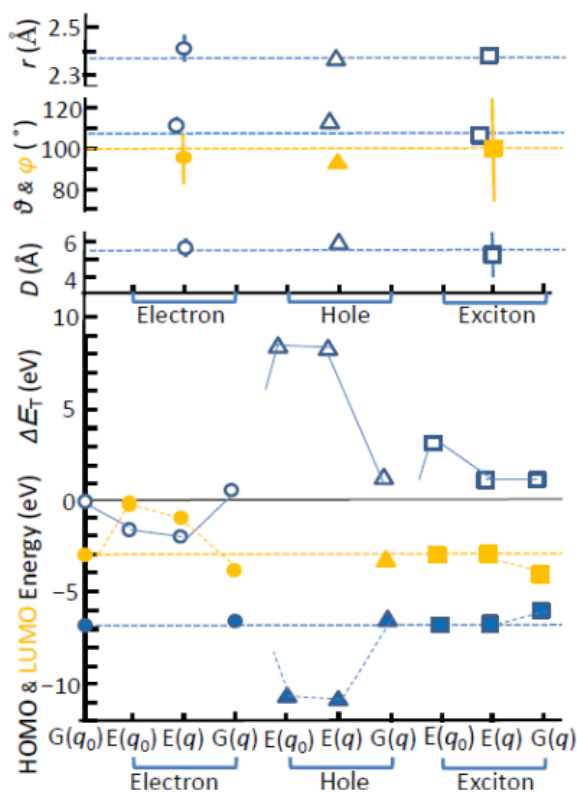


Fig. 3. Addition effects of an electron ( $\circ$ ), hole ( $\Delta$ ), and exciton ( $\square$ ) to  $G(q_0)$  (dotted lines) in  $\text{Se}_3$  at the states of  $E(q_0)$ ,  $E(q)$  and  $G(q)$ . From the top toward the bottom, plotted are the bond length  $r$ , bond angle  $\theta$  (open symbols) and dihedral angle  $\varphi$  (solid symbols), ring diameter  $D$ , the total-energy change  $\Delta E_T$  (open symbols) from the initial  $E_T(q_0)$  value, and electronic energies (HOMO and LUMO levels for neutral states or half-filled outermost levels in the charged states) (solid symbols). Bars in  $\varphi$  denote the variations, not errors.

Hole and exciton additions also produce notable changes. Comparing the three excitations, we see that the exciton causes the most conspicuous shape change, the electron the next, and the hole the smallest. For instance, as shown in Fig. 3, the deformation induced by an exciton is drastic with  $D = 4.01$  and  $6.35$  Å. On the other hand, a marked difference from the electron case is that the hole and the exciton addition increase (de-stabilize) the total energy,  $\Delta E_T > 0$ , which may be due, respectively, to reduction in the electron number and to structural disordering as inferred from the scattered (long bar)  $\varphi$  in

Fig. 3. Besides, the hole addition accompanies substantial energy decrease in the half-filled outermost (originally HOMO) state, which suggests weakened interaction between LP electrons. On the other hand, a common feature to the three is that all the induced changes recover to the initial states after deexcitation and structural relaxation;  $q \rightarrow q_0$  along the  $G$  curve in Fig. 1.

It may be interesting to compare the present excitonic (illumination) effect with that obtained by Hoshino et al. [12] using an *ab initio* MD simulation. A notable difference is that, upon excitation, the MD simulation manifests no steady states and also spontaneous breakage ( $r > 2.7$  Å) of some bond, while in the present MO calculation no bond breaking occurs despite of the marked ring deformations. It should be mentioned here that they demonstrate such bond scission also for 14Se chains connected with the repeated boundary condition. (Such a behavior is contrastive to the present results, while it is similar to the behavior in constraint chains, as will be described in Sections 3.2 and 3.3.) Reasons of these differences may be ascribed to prefixed temperatures; 500 K (higher than the melting temperature of Se, 490 K [28]) in the MD simulation and formally 0 K in the MO calculation. We should also note that their results delineate structural changes *during* excited states of 1 ps, and accordingly, no insights into structural relaxation *after* electron-hole recombination have been obtained.

### 3.2. Free single chains

How is the excitation effect different in chain clusters? To examine the feature, we construct energy-optimized H- $n$ Se-H chains with  $n = 2 - 10$  in a similar way to the previous study [26, 27]. The shape is helical with  $r = 2.37$  Å,  $\theta \approx 107^\circ$ , and  $\varphi \approx 83^\circ$ , which are comparable with experimental results of single Se chains in zeolite pores [8-10] and theoretical ones [12, 15, 16];  $r = 2.3 - 2.5$  Å,  $\theta = 99 - 121^\circ$ , and  $\varphi = 42 - 82^\circ$ . Note that the dihedral angle in isolated Se chains is appreciably smaller than that  $\varphi \approx 102^\circ$  (with  $r = 2.36$  Å and  $\theta = 104^\circ$ ) in trigonal (t-) Se [28, 29], the difference being ascribable to interchain interaction.

Fig. 4 exemplifies electron-addition effects in the H-5Se-H chain, with related parameters included in Fig. 5. Fig. 4(a, a') shows the energy-optimized initial structure, in which the edge-to-edge Se distance  $L$  is 6.32 Å,  $E_{\text{HL}} = 3.86$  eV (Fig. 5e), and  $E_T = -12007.068$  H, the last being taken as a reference.

The electron addition yields marked changes. The total energy is lowered by  $\sim 1$  eV, i.e. the cluster becoming more stable in a similar way to that of the ring. The original LUMO level with the wavefunction of Fig. 4(a') is now half-filled, and the energy rises by  $\sim 3$  eV. Then, successive structural relaxation ( $q_0 \rightarrow q$ ) produces an electron polaron with  $E_p = 0.65$  eV (Fig. 5d) and lowers the half-filled level by 1.35 eV, which may be consistent with a recent MD result [14]. Concomitantly, as shown in Fig. 4(b, b'), the short-range structure considerably deforms to  $r \approx 2.47$  Å,  $\theta \approx 122^\circ$  and  $\varphi \approx 104^\circ$  (Fig. 5a, b), resulting in chain

lengthening  $\Delta L/L (= L(q - q_0)/L(q_0))$  amounting to  $\sim 30\%$  (Fig. 5c), in qualitative agreement with an MD result by Hegedüs et al. [13], which is assumed to be caused by Coulombic repulsive forces. Such results may predict that, upon electron irradiation, trigonal Se whiskers and also isolated Se chains elongate, working as charge-controlled atomic springs. Next, deleting the electron ( $E \rightarrow G$  at  $q$ ) gives a neutral state with a markedly narrowed  $E_{\text{HL}}$  of  $\sim 2.5$  eV (Fig. 5e), the origin being discussed later. However, successive structural relaxation with the energy optimization process has recovered the initial state,  $q \rightarrow q_0$ , the electron effect being the transitory type in Fig. 1.

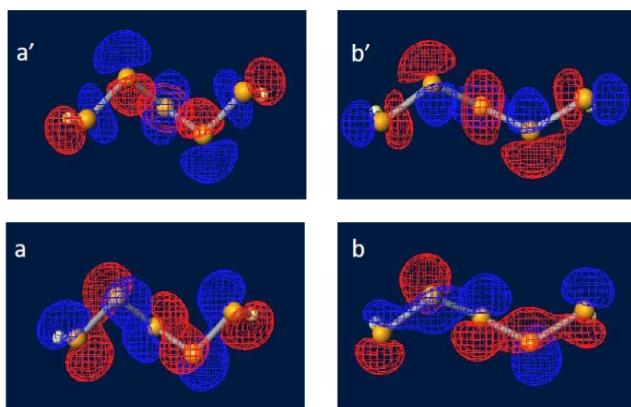


Fig. 4. H-5Se-H chain with the LUMO (upper) and HOMO (lower) wavefunctions at (a, a') the initial  $G(q_0)$  and (b, b') the electron-induced  $G(q)$ .

Circles in Fig. 5 plot variations of the electron effects in H- $n$ Se-H as a function of  $n$ . Fig. 5(a, b) show the short-range parameters ( $r$  and  $\theta$ ) and  $\varphi$  at the initial configuration  $q_0$  and the polaronic  $q$ ; the results manifesting maximal modifications of  $r$ ,  $\theta$  and  $\varphi$  at the corresponding smallest  $n$ 's ( $= 2, 3$  and  $4$ , respectively) and reductions toward the  $q_0$  values with increasing  $n$ . Actually, H-2Se-H undergoes a dramatic  $r$  increase from 2.37 to 3.09 Å; the Se-Se bond being practically cut. And, angular widenings at  $n = 3$  and  $4$  amount, respectively, to  $\theta = 147^\circ$  and  $\varphi = 121^\circ$  (from  $108^\circ$  and  $83^\circ$ ). We also see in Fig. 5(d) that the polaronic energy  $E_p$  and the total-energy change  $\Delta E_T(q \rightarrow q_0)$  in the ground state also exhibit similar  $n$  dependences, with the maxima of  $\sim 1.5$  eV at  $n = 2$ , which are followed by monotonic decreases toward zero with increasing  $n$ . These features are attributable to more localized Coulombic effects in shorter chains.

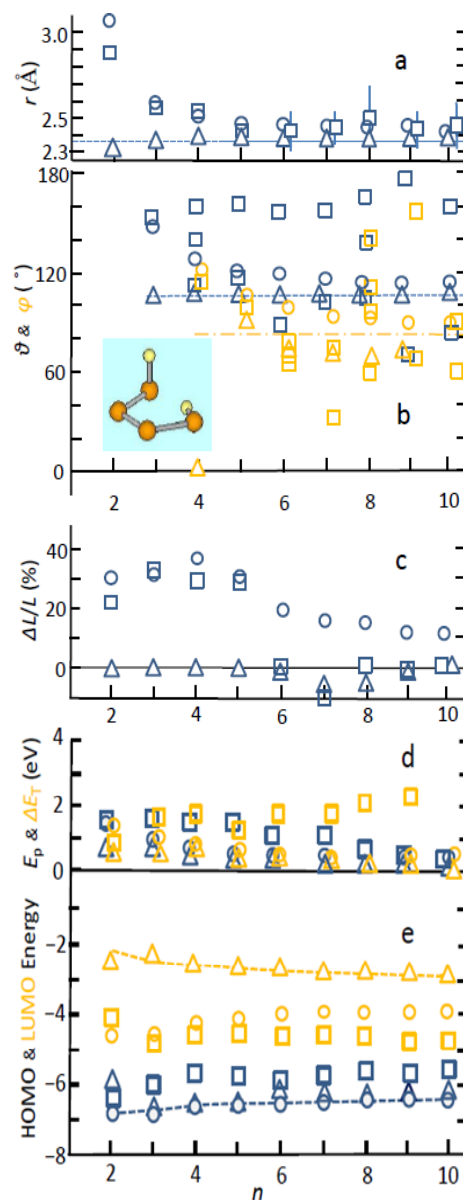


Fig. 5. Addition effects of an electron ( $\circ$ ), hole ( $\Delta$ ) and exciton ( $\square$ ) on structural and electronic parameters in H- $n$ Se-H chains as a function of  $n$ ; from the top toward the bottom, (a) the Se-Se bond distances  $r(q_0)$  (dashed line) and  $r(q)$  (symbols), (b) bond angles  $\theta(q_0)$  (dotted line) and  $\theta(q)$  (blue symbols), dihedral angles  $\varphi(q_0)$  (dot-dashed line) and  $\varphi(q)$  (orange symbols) with the inset showing the deformed H-4Se-H by a hole, (c) the fractional length changes  $\Delta L(q - q_0)/L(q_0)$  of the total Se chain length (between the terminal Se atoms), (d) the polaronic energy  $E_p$  (the difference in  $E_T$  at  $E(q_0)$  and  $E(q)$ , blue) and the difference  $\Delta E_T$  in total energy at  $G(q)$  and  $G(q_0)$  (orange), and (e) HOMO (blue) and LUMO (orange) energies in the initial state  $G(q_0)$  (dotted lines) and at  $G(q)$  (symbols). In (a, b, d), the symbols are horizontally shifted a bit for evading overlapping. Bars in (a) denote variations, not errors.

Nevertheless, Fig. 5(c) shows that the fractional chain elongation  $\Delta L/L$  exhibits a maximum at  $n = 4$ , the reason attracting some consideration. It seems to result from counterbalance between electronic and lattice forces. We here approximate a helical Se chain as a columnar rod with a length  $L$ , a cross section  $S$ , and an elastic constant  $k$ , and suppose that it is subjected to an elongation force  $F$ . We then have  $\Delta L/L = F/(kL)$ , which leads to  $\Delta L/L \sim 1/L$ , provided that  $F$  and  $k$  are independent of  $L$ , in consistency with the monotonic decrease at  $n \geq 4$ . Actually, a simple Coulombic calculation for the rod with a dielectric constant of  $\epsilon$  having a uniform charge  $Q$  derives  $F = Q^2/(2\epsilon S)$ , being independent of  $L$ . However, we should note that  $k$  in the helical chain varies with  $n$ . For instance, the valence-force field model for t-Se demonstrates  $k_r > k_\theta$  ( $k_r$  and  $k_\theta = 1.2$  and  $0.14 \times 10^5$  dyn/cm [30]) and probably  $k_\theta > k_\phi$ , where  $k_r$ ,  $k_\theta$  and  $k_\phi$  are the force constants for  $r$ ,  $\theta$ , and  $\phi$  variations. Such magnitude relations may hold also in isolated Se chains [23], and accordingly, the elastic property of the chains with  $n = 2, 3$  and  $\geq 4$  is probably governed by  $k_r$ ,  $k_\theta$  and  $k_\phi$ , respectively, which explains the increase in  $\Delta L/L$  from  $n = 2$  to 4.

Fig. 5(e) shows variations of the HOMO and LUMO energies with  $n$ . We see that  $E_{\text{HL}}$  at  $G(q_0)$  (dashed lines) becomes narrower with increasing  $n$ , as demonstrated previously [27], which arises from extension of relevant wavefunctions.

On the other hand, the HOMO and LUMO energies at  $G(q)$  upon electron addition ( $\circ$ ) possess contrastive features. These are similar to and lower by  $\sim 3$  eV than those of the initials, irrespective of  $n$ 's. This result seems to manifest different origins of the HOMO and the LUMO level,  $\pi^*$  and  $\sigma^*$ , the latter being strongly dependent upon  $r$ . Its lengthening, plotted in Fig. 5(a), by the Coulombic repulsion weakens the covalent bond, reducing the energy separation between  $\sigma$  and  $\sigma^*$  states, which lowers the LUMO level. On the contrary, as shown in Fig. 4, the LP wavefunction is more extended and scarcely affected by  $r$ . These circumstances result in the nearly  $n$ -independent  $E_{\text{HL}}$  ( $\approx 3$  eV) at the  $G(q)$  state. Lastly, it should be noted that, despite of these marked polaronic effects, all the transformations appear to be transitory,  $q \rightarrow q_0$ .

Fig. 5 also displays addition effects of a hole ( $\Delta$ ). We first note for Fig. 5(a, b) negligible hole-induced changes in  $r$  and  $\theta$ , which are consistent with the fact that the covalent bond is hardly affected by the hole addition to the HOMO state. By contrast, the hole exerts notable changes upon  $\phi$ . Different from the electron case, the hole reduces LP-LP interaction and tends to make the helical chains planar,  $\phi(q_0) > \phi(q)$ , in consistency with an empirical MO result [17]. For instance, in H-2Se-H, the initial trans-conformation has changed to a planar structure at the polaronic state  $E(q)$ ; i.e.,  $\phi_{\text{H}}$  (the dihedral angle for H) changing from  $90^\circ$  to  $0^\circ$  (not shown), making the Se LP wavefunctions parallel, which gives rise to slight  $r$  shortening from 2.37 to 2.32 Å (Fig. 5(a)). The paralleled LP wavefunctions of the Se atoms are retained at  $G(q)$ , in which induced repulsive LP-LP interaction seems to be

responsible for a noticeable rise in the HOMO level by  $\sim 1$  eV (Fig. 5(e)). Such a conformational change is conspicuous also in H-4Se-H, as seen from a dramatic  $\phi$  decrease from  $86^\circ$  to  $2^\circ$ , shown in the inset Fig. 5(b), which is attributable again to the reduced LP-LP interaction. And, Fig. 5(b) suggests that the interaction, which makes  $\phi$ 's smaller or segments planar, extends over  $\sim 7$  atoms. Since  $L$  is written as [15];

$$L = nr\{(1 - \cos\theta - \cos\phi + \cos\theta\cos\phi)/(3 + \cos\theta - \cos\phi + \cos\theta\cos\phi)\}^{1/2},$$

we obtain  $\partial L/\partial\phi > 0$ , which suggests that the smaller  $\phi$ 's are likely to cause the negative  $\Delta L/L$  at  $n \approx 7$  in Fig. 5(c). On the other hand, Fig. 5(d, e) show that  $E_{\text{p}}$ ,  $\Delta E_{\text{T}}$  for  $G(q \rightarrow q_0)$ , and energy modifications of HOMO and LUMO levels by hole addition are the smallest among the three excitations, which are ascribable to the extended  $\pi$ -type LP wavefunction. Finally, it should be pointed out that all the transformations are transitory, except that for  $n = 2$ , in which case the LP-LP repulsion produces the quasi-stable state ( $G(q')$  in Fig. 1) with  $r = 2.43$  Å.

Exciton effects ( $\square$ ) appear to be complicated, but for H-2Se-H, and the whole process cannot be delineated with two reasons. One is that the iterated optimization calculation from  $E(q_0)$  toward  $E(q)$  has been abnormally terminated at the instant when the excited-state total energy relaxes to the same value with a rising ground-state energy,  $E_{\text{T}}(E(q)) = E_{\text{T}}(G(q))$ , or when  $E_{\text{PL}} = 0$ ; the result suggesting that the exciton will ultimately be self-trapped. Only the behavior of H-2Se-H could be analyzed successfully, with the parameters shown in Fig. 5, and the deformed structure recovers to the initial. For H- $n$ Se-H chains with  $n \geq 3$ , we then regard the energy-coincidental point as  $q$ , which makes the results plotted in Fig. 5 tentative. The other, which may be related with marked chain flexibility under excitonic excitations and/or the B3LYP/6-31+G\* calculation, is that the optimization process has depended critically upon programming details such as employed atom coordinates (internal or Cartesian) and atom indexing. For instance, for the chains with  $n = 5$  and 6, there seem to exist stable and quasi-stable polaronic structures, which finally relaxes to ground-state structures having a linear segment (Fig. 6(d)) and an IVAP (intimate valence-alternation pairs) (Fig. 6(d')), the latter being higher (unstabler) in energy by  $\sim 1$  eV. Hence, Fig. 5 plots parameters of the stablest configurations. Besides, it is mentioned that,  $E_{\text{T}}(G(q'))$  for H-10Se-H could not be calculated with unknown reasons.

Regarding the exciton effects in the H- $n$ Se-H chains, we mark four features. First, as shown in Fig. 5(a), with an increase in  $n$  from 2,  $r(q)$  tends to approach from 2.85 Å to the initial value 2.37 Å, in a similar way to the electron case. Nevertheless, we see appreciable scatterings of  $r$ ,  $\theta$  and  $\phi$  at  $n \approx 8$ , which imply that the exciton adds substantial structural disorder to the helical chain. Second, Fig. 5(c) shows a sign reversal of  $\Delta L/L$  at around  $n = 6$ . Below 5 and above 6,  $\Delta L/L$  resembles those of the electron and the hole, respectively. At  $n = 7$ ,  $\Delta L/L$  manifests a minimum, which

may be connected with the smallest  $\varphi$  ( $\approx 32^\circ$  and  $77^\circ$ ). Third, we see in Fig. 5(e) that, irrespective of  $n$ ,  $E_{\text{HL}}$  at  $G(q)$  is the narrowest (1 – 2 eV) among those of the three excitations, the result arising from the higher HOMO levels than the others and the comparable LUMO levels with those of the electron. The higher HOMO and lower LUMO levels than the initials are ascribable to stronger LP and weaker  $\sigma$  interactions, respectively, both of which may be related with the structural disordering. Fourth, in H-9Se-H, the helical chain has relaxed to an  $\Omega$ -shape conformation with a diameter of  $\sim 7$  Å at  $G(q')$ . However, it should be noted that, except this chain (and the cluster containing an IVAP), the structural transformations are transitory.

How can we understand these seemingly complicated variations of the exciton effects? A close inspection of deformed shapes at the polaronic states  $q$  in the clusters of  $n \geq 3$  points out a common, unique bond connection, i.e., a fairly straight -Se-Se-Se- sequence with  $\theta \approx 170^\circ$  (Fig. 5(b)). In H-3Se-H only the straight unit appears, and in H-4Se-H, an edge atom is connected to the adjacent with  $\theta = 110^\circ$ . In the chains of  $n \geq 5$ , the connection has two edge atoms with  $\theta \approx 100^\circ$  (see, Fig. 6(d)), and the structure causes the sign reversal of  $\Delta L/L$  at  $n \approx 6$  (Fig. 5(c)).

Why does such a straight three-atom unit appear upon exciton excitations? Or, more fundamentally, why does the normal Se chain take a helical form with  $\theta \approx \varphi \approx 90^\circ$  [28]? For this problem, Ikawa and Fukutome have proposed that  $\theta \approx 90^\circ$  arises from the two, orthogonally-coordinated p-type  $\sigma$ -bonds, and  $\varphi \approx 90^\circ$  is governed by the interaction between a  $\pi$ -type LP wavefunction and parallel p-type  $\sigma$ -bonds of the two adjacent atoms (as illustrated in Fig. 7 in Ref. 16). Such an idea suggests that, upon formation of an exciton, which may extend over 5 – 6 atoms, the  $\sigma$  and  $\pi$  states are conjugated. And, the conjugation makes the straight connection energetically favorable, in which the shape is governed by a single p-wavefunction of the center atom of the -Se-Se-Se- sequence. However, some strains and residual charges are likely to accumulate at the edges, which seems to cause the nearly-orthogonal bond angles.

Finally, comparisons of gross features in the  $\text{Se}_8$  ring and the H- $n$ Se-H chains may be interesting. We notice a similar trend, i.e. an electron and an exciton exert prominent changes while a hole causes relatively minor effects, the reason being attributable to the spatially localized  $\sigma^*$  and fairly extended LP wavefunctions. Nevertheless, for the three excitations, the free helical chain tends to undergo more conspicuous changes than those in the  $\text{Se}_8$  ring, probably because of no closure constraint. For instance, in the H-8Se-H chain, the electron addition causes the  $r$  increase to  $\sim 2.43$  Å, which is substantially greater than  $\sim 2.39$  Å in the  $\text{Se}_8$  ring.

### 3.3. Constrained single chains

For a-Se, we would envisage that the conformation of segmental chains is restricted in some degrees by peripheral structures. It is then plausible that the segment arrangement practically takes a form in between the free and constrained

configurations. Accordingly, we here examine responses of the latter using H- $n$ Se-H ( $n = 3, 5$  and  $7$ ) clusters, in which the positions of two Se atoms at both edges are fixed. Note that similar results have been obtained under H-fixing, instead of the Se-fixing.

Fig. 6(b', c', d') exemplifies the polaronic configurations in the H-5Se-H produced by the three excitations, under the terminal Se-Se distance being fixed at the initial value of 6.32 Å. We see that, roughly, the three behaviors resemble those of the free chains. The electron addition lengthens  $r$  to 2.4 – 2.6 Å in Fig. 6(b'). The hole addition gives the slightest change also in the constrained case, as shown in the similar shapes of Figs. 6(a, c, c'). By contrast, the exciton addition shown in Fig. 6(d') provides a conspicuous structural change, including bond breakage ( $r = 3.40$  Å) and angular scattering of  $\theta \approx 73^\circ - 114^\circ$ . Since the terminal Se atoms are fixed, greater strains would appear in the intra-cluster parameters. (Note, however, that this result is tentative, due to the abnormal optimization termination, in a similar way to the free-chain cases.) Lastly, it should be underlined that all the deformed structures recover to the initial,  $q \rightarrow q_0$ , which is possibly assisted by the fixed Se-Se distances.

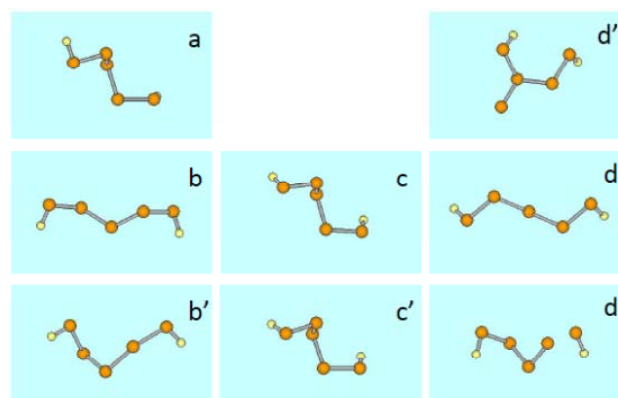


Fig. 6. Conformation variations of a H-5Se-H chain: (a) initial  $q_0$ , (b, b') electron-, (c, c') hole- and (d, d') exciton-polaron structures in the free (b, c, d) and the length-fixed clusters (b', c', d'). (d'') shows a quasi-stable excitonic polaron.

### 3.4. Se-chain dimers

How are the excitation effects in chain assemblies held together by inter-cluster forces? It is plausible that in a-Se (and t-Se) the inter-chain interaction plays crucial roles, while the effects would necessarily vary with chain structures, which can take a variety of intra- and inter-chain conformations. Under the circumstances, as the simplest example, we here examine behaviors of the most stable dimer structures consisting of H-2Se-H clusters.

Fig. 7(a) shows the dimer with the HOMO and LUMO wavefunctions. This initial conformation has been obtained through energy-optimization calculations of several *ad hoc* structures. Actually, this arrangement has a smaller total energy ( $= -9607.0479$  H) than those of the two isolated H-2Se-H clusters by  $\sim 50$  meV. The intrachain structure ( $r = 2.38$  Å,  $r_{\text{H}} = 1.49$  Å,  $\theta_{\text{H}} = 97^\circ$ ,  $\varphi_{\text{H}} = 89^\circ$ ) is practically

the same with that in the single chain ( $r = 2.37$  Å,  $r_H = 1.49$  Å,  $\theta_H = 97^\circ$ ,  $\varphi_H = 90^\circ$ ). Regarding the interchain correlation, both the two Se-Se bonds and the two inner and outer Se-H bonds align in parallel, with the nearest and farthest distances between Se atoms being 3.56 and 8.03 Å. We also see in the figure that the HOMO and LUMO states have  $\pi^*$ - and  $\sigma^*$ -type wavefunctions, respectively, in consistent with the known idea [1-3]. And, as shown in Fig. 8, the dimer has  $E_{HL} = 4.31$  eV, which is compared with those in the single H-2Se-H (4.69 eV) and H-4Se-H (4.00 eV) chains in Fig. 5.

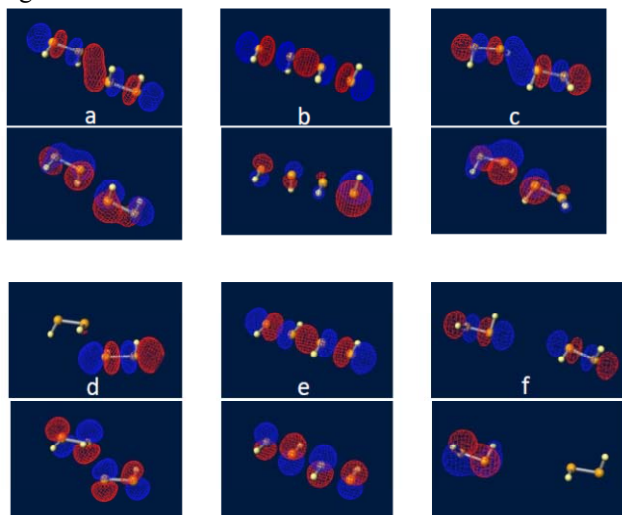


Fig. 7. HOMO (lower) and LUMO (upper) wavefunctions of (a) an energy-optimized H-2Se-H dimer and excitation-induced changes: (b) and (c) show the electron effects at  $G(q)$  and  $G(q')$ , (d) the hole at  $G(q)$ , and (e) and (f) the exciton at  $G(q)$  ( $= E(q)$ ) and  $G(q')$ .

The electron addition induces the following changes: First, for the vertical transfer in Fig. 1, the LUMO shape at  $G(q_0)$  is retained in the outermost wavefunction at  $E(q_0)$ , while the energy increases by  $\sim 2$  eV and  $E_T$  decreases by  $\sim 1$  eV (Fig. 8). Then, as shown in Fig. 7(b), from  $E(q_0)$  to  $E(q)$ , the cluster relaxes with  $E_p \approx 0.92$  eV (Fig. 8), in a similar way to that in single H-2Se-H ( $E_p \approx 1.44$  eV, Fig. 5(d)). The Se-Se separations are now increased to 2.73 – 2.82 Å (Fig. 8), and all the Se atoms align in straight with extension of the end-to-end Se-Se distance to 8.29 Å, which is consistent with instantaneous volume expansions upon electron additions, demonstrated in the MD simulation [13]. Such structural changes are again attributable to the Coulombic repulsive force produced by the electron. This  $r$  lengthening makes the covalent bonds weaker, which causes marked lowering of the LUMO level (to  $-4.53$  eV, Fig. 8) at the strained neutral state  $G(q)$ . Successive structural relaxation transforms the dispersed structure to the configuration  $G(q')$  in Fig. 7(c), the shape being slightly different from the initial, while  $\Delta E_T \approx 0$  eV reflecting the weak van-der-Waals potential.

On the other hand, the hole produces more-or-less conspicuous inter-cluster changes. As shown in Figs. 7(a, d), from  $q_0$  to  $q$  with  $E_p \approx 0.63$  eV (Fig. 8), the H positions have

been rotated to  $\varphi_H \approx 33^\circ$ , which tends to couple intrachain LP wavefunctions in each H-2Se-H. (The rotating direction is the same as the single chain, but magnitude being smaller.) More important may be the facts that the hole couples the interchain LP wavefunctions and also aligns the two chains. It is plausible that such chain-coupling alignment preludes the photo-crystallization in a-Se, which has been demonstrated to be induced by holes [31]. The nearest and farthest interchain Se-Se distances are now reduced to 3.29 and 7.03 Å (from 3.56 and 8.03 Å), which may cause the transitory volume contraction, also demonstrated in the MD analysis [13]. However, deleting the hole and relaxing the structure recovers the initial conformation, Fig. 7(a).

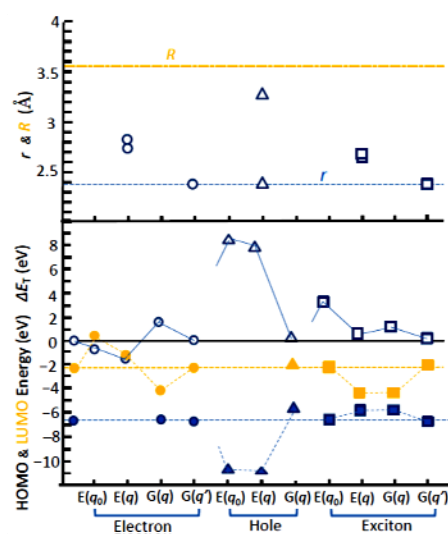


Fig. 8. Electron- ( $\circ$ ), hole- ( $\Delta$ ) and exciton-addition ( $\square$ ) effects in a H-2Se-H dimer at  $G(q_0)$  (dotted lines),  $E(q_0)$ ,  $E(q)$ , and  $G(q)$  (and  $G(q')$ ) for electron and exciton. From the top to the bottom, the nearest inter-cluster distance  $R$  and the bond length  $r$ , the total-energy change  $\Delta E_T$  (open symbols) from the  $G(q_0)$  value, and HOMO and LUMO (or half-filled outermost state) energies (solid symbols).  $E_p$  is given as  $\Delta E_T$  between  $E(q_0)$  and  $E(q)$ .

Finally, we see in Fig. 7(e, f) that the exciton effect resembles the electron effect, Fig. 7(b, c). From  $G(q_0)$  to  $E(q_0)$ , the HOMO and LUMO wavefunctions retain the shapes, while  $E_T$  increases by  $\sim 3$  eV ( $= E_{PLE}$ ). From  $E(q_0)$  to  $E(q)$  with  $E_p = 1.28$  eV, the four Se atoms align straight with  $r = 2.67$  and 2.70 Å, which slightly lengthens the end-to-end Se-Se distance to 8.03 Å (Fig. 7(e)). Such a dismembering state may be responsible for the photoinduced fluidity appearing in a-Se [32, 33] (and also in g-As<sub>2</sub>S<sub>3</sub> [1, 2]) during illumination. After exciton recombination, the structure relaxes to an isolated-chain conformation  $G(q')$  (Fig. 7(f)) with  $\Delta E_T \approx +0.035$  eV and  $E_{HL} \approx 4.65$  eV. The structural change from Fig. 7(a) to (f) can cause the memorable volume expansion, experimentally detected [34].

### 3.5. P-like conduction, photoluminescence and photoinduced phenomena

It has long been known that almost of all covalent chalcogenide glasses exhibit p-like behaviors [4]. For instance, the drift mobility  $\mu_d$  in a-Se at room temperature are reported to be  $\sim 0.15$  and  $\sim 0.005$  cm<sup>2</sup>/Vs for holes and electrons [28]. However, the p-like reason remains controversial, which has been ascribed to the extended LP states [35], polarons [36], and intrinsic defects [37]. In this context, it may be worthwhile to recall that, also in t- and  $\alpha$ -monoclinic Se crystals, the latter being composed by stacked Se<sub>8</sub> rings, holes are more mobile than electrons [28]. Note that this observation for t-Se is seemingly contrastive to a heavier effective hole mass theoretically predicted on rigid-lattice models [38, 39]. Then, taking the Drude formula  $\mu = e\tau/m^*$  ( $\tau$  and  $m^*$  are the carrier-phonon relaxation time and the effective mass) into account, we would assume  $\tau_e < \tau_h$  in t-Se. But, how can we understand this inequality?

Alternatively, the present calculation demonstrates for all the studied clusters that the carriers accompany deformations of atomic structures. And, the electron is more polaronic. Actually, we have seen in Figs. 3, 5 and 8 (for Se<sub>8</sub> ring, H-*n*Se-H, dimer) that  $E_p$  for electrons ( $= 0.41, < 1.5, 0.92$  eV) is greater than that for holes ( $= 0.19, < 0.7, 0.63$  eV). Since the polaron mass  $M$  increases with  $E_p$  through some functional forms as  $M \sim \exp(E_p/\hbar\Omega)$  [40], where  $\hbar\Omega$  is a vibrational energy, the electron-hole  $E_p$  relation could be interpreted equivalently to  $M_e > M_h$ . We then expect that the less-polaronic, lighter  $M_h$  governs the p-like conduction in a-, t-, and  $\alpha$ -monoclinic Se. Specifically, for the thermal activation energy  $E_a$  of  $\mu_d(T)$  in a-Se, Dolezalek and Spear obtained  $\sim 0.30$  and  $\sim 0.25$  eV for electrons and holes [41], which appears to be in harmony with the  $E_p$  ( $\sim 2E_a$ ) values. Note that the polaron model can provide a plausible interpretation of avalanche breakdown in a-Se [42]. We also add that this model is consistent with n-like conduction in GeSe<sub>2</sub> and many oxide materials including SiO<sub>2</sub> [3], in which the lattices are three-dimensionally rigid so that polaronic deformations can practically be neglected.

It has also been known that the chalcogenide glass exhibits photoluminescence at around the half-gap energies [2, 3, 5]. As<sub>2</sub>S(Se)<sub>3</sub> glasses follow the observation, for which several ideas including the charged defect model have been proposed [2, 3, 5]. However, in details, the luminescence in a-Se is located at clearly smaller energy than the half gap [3, 5]; the photoluminescence peak energy  $E_{PL}$  normalized by the excitation-spectrum peak energy  $E_{PLE}$  being  $\sim 0.4$ , for which interpretations remain. Interestingly, t-Se also exhibits a similar ratio,  $E_{PL}/E_{PLE} \approx 0.4$  [43].

In the present scope, we expect that excitons cause the photoluminescence, with the energy ratio of  $E_{PL}(q)/E_{PLE}(q_0)$ . Table 1 lists related parameters for the clusters of interest. We see in the table  $E_{PL}(q)/E_{PLE}(q_0) \approx 0.2 - 0.4$ , which is consistent with the observed sub-halfgap luminescence spectrum. That is, the  $E_{PL}/E_{PLE}$  ratio could be interpreted as a manifestation of strong polaronic interaction. In other clusters, not listed in Table 1, the exciton seems to be self-trapped, i.e.,  $E_{PL}(q) < 0$ , and accordingly, those are practically unable to emit luminescence. Or, the present

result may predict that, in a-Se, only ring(-like) connections and short segments are responsible for photoluminescence.

Table 1. The HOMO-LUMO gap energy  $E_{HL}$ , the exciton-excitation energy  $E_{PLE}$ , and the exciton recombination energy  $E_{PL}$  at the initial  $q_0$  and the polaronic  $q$  state (in unit of eV), with the ratios  $E_{HL}(q)/E_{HL}(q_0)$  and  $E_{PL}(q)/E_{PLE}(q_0)$  for Se<sub>8</sub>, H-2Se-H, and H-2Se-H dimer.

cluster	$E_{HL}(q_0)$	$E_{PLE}(q_0)$	$E_{HL}(q)$	$E_{PL}(q)$	$E_{HL}/E_{HL}$	$E_{PL}/E_{PLE}$
Se <sub>8</sub>	3.83	2.98	1.98	1.09	0.52	0.37
H-2Se-H	4.69	3.59	2.29	1.15	0.49	0.32
dimer	4.31	3.48	1.43	0.52	0.33	0.15

Finally, regarding the excitation-induced phenomena, the present results have demonstrated unique effects of the three species. An electron and an exciton tend to produce gross intra-cluster structural changes, which may cause the fluidity and the volume expansion *during* the excitations [1-3]. The electron effect may also be related with suppression of the nucleation rate of crystallization under electron-beam irradiation [44]. On the other hand, the hole appears to enhance inter-cluster correlation, which can work as motive forces triggering the photocrystallization [31].

However, further studies remain for interpreting photoinduced memory effects. Actually, in many cases, except a few exciton effects, induced polaronic deformations have relaxed to the initial structure, which cannot afford the memory effects, including photodarkening (nearly parallel red-shifts of optical absorption edges, induced by illumination and recovered with annealing at glass-transition temperatures), in a-Se and similar memorable photo-effects in isolated Se chains [8-10]. We may then need more advanced analyses for excitonic effects in disordered and/or entangled clusters. Nevertheless, MD calculations tend to confront time limitations in simulating such phenomena [2, 11-13]. Accordingly, for understanding the memory effects, we may prefer MO procedures. In addition, for studying vector (light-polarization dependent) photoinduced phenomena [1-3], we should analyze explicitly the electron-light interaction in clusters of interest.

## 4. Conclusions

To understand unique electronic properties of chalcogenide glasses, we have studied the addition effects of an electron, hole, and exciton to crown-shaped Se<sub>8</sub> and several helical H-*n*Se-H clusters through *ab initio* MO calculations. Marked results can be summarized as follows: i) Excitation-induced structural and electronic changes in Se<sub>8</sub> are relatively moderate, probably due to constraint of the ring structure. ii) In free H-*n*Se-H clusters, the excitations produce

conspicuous, polaronic changes, which arise from counterbalance between electronic forces and lattice rigidity. Electron addition causes prominent changes in short ( $n \leq 5$ ) chains, a hole induces milder modifications, and exciton effects in the clusters with  $n \leq 5$  and  $\geq 6$  resemble those of an electron and a hole, respectively. When the excitation is taken away, the cluster tends to recover to the initial state, with some exceptions.

iii) In the clusters, with the total length being fixed, excitation effects are likely to become moderate, reflecting the constraint.

iv) In an energy-optimized H-2Se-H dimer, an electron and an exciton behave similarly, including cluster dismembering and irreversible structural changes. By contrast, a hole couples the two chains, enhancing inter-chain correlation.

v) The present results provide fundamental insights into the origins of the p-like conduction, sub-halfgap photoluminescence spectrum, photo-crystallization, and photo-fluidity in a-Se. These features are governed by the  $\pi^*$ -type HOMO and  $\sigma^*$ -type LUMO states, which form the valence- and conduction-band edges in Se solids.

## References

- [1] M. A. Popescu, *Non-Crystalline Chalcogenides*, (Kluwer Academic Pub., Dordrecht, 2000).
- [2] A.V. Kolobov (ed.), *Photo-Induced Metastability in Amorphous Semiconductors*, (Wiley-VCH, Weinheim, 2003).
- [3] K. Tanaka, K. Shimakawa, *Amorphous Chalcogenide Semiconductors and Related Materials*, (Springer, New York, 2011).
- [4] S. Kasap, J.F. Frey, G. Belev, O. Tournant, H. Mani, J. Greenspan, L. Laperriere, O. Bubon, A. Reznik, G. DeCrescenzo, K.S. Karim, J. A. Rowlands, *Sensors* **11**, 5112 (2011).
- [5] K. Tanaka, *J. Optoelectron. Adv. M.* **15**, 1165 (2013).
- [6] K. Nagaya, T. Hayakawa, M. Yao, H. Endo, *J. Non-Cryst. Solids* **205-207**, 807 (1996).
- [7] C. Bréchnac, Ph. Cahuzac, N. Kébaïli, J. Leygnier, *J. Chem. Phys.* **112**, 10197 (2000).
- [8] Y. Katayama, M. Yao, Y. Ajiro, M. Inui, H. Endo, *J. Phys. Soc. Jpn.* **58**, 1811 (1989).
- [9] A. Goldbach, M.-L. Saboungi, *Acc. Chem. Res.* **38**, 705 (2005).
- [10] A. Saitoh, H. Takebe, K. Tanaka, *J. Optoelectron. Adv. M.* **13**, 1524 (2011).
- [11] X. Zhang, D.A. Drabold, *Phys. Rev. Lett.* **83**, 5042 (1999).
- [12] K. Hoshino, F. Shimojo, T. Nishida, *J. Phys. Soc. Jpn.* **68**, 1907 (1999).
- [13] J. Hegedüs, K. Kohary, D.G. Pettifor, K. Shimakawa, S. Kugler, *Phys. Rev. Lett.* **95**, 206803 (2005).
- [14] K. Prasai, P. Biswas, D.A. Drabold, *Semicond. Sci. Technol.* **31**, 073002 (2016).
- [15] M. Springborg, R.O. Jones, *J. Chem. Phys.* **88**, 2652 (1988).
- [16] A. Ikawa, H. Fukutome, *J. Phys. Soc. Jpn.* **58**, 4517 (1989).
- [17] A. Ikawa, H. Fukutome, *J. Phys. Soc. Jpn.* **59**, 1002 (1990).
- [18] T. Uchino, S.R. Elliott, *Phys. Rev. B* **67**, 174201 (2003).
- [19] J. Berashevich, A. Mishchenko, A. Reznik, *Phys. Rev. Appl.* **1**, 034008 (2014).
- [20] M. Shpotyuk, M. Hyla, O. Shpotyuk, V. Gurin, *Computational Mater. Sci.* **113**, 112 (2016).
- [21] T. Takahashi, K. Ohno, Y. Harada, *Phys. Rev. B* **21**, 3399 (1980).
- [22] K. Tanaka, *Solid State Commun.* **4**, 867 (1985).
- [23] K. Nakamura, A. Ikawa, *Phys. Rev. B* **67**, 104203 (2003).
- [24] M. W. Schmidt, K. K. Baldrige, J. A. Boatz, S. T. Elbert, M. S. Gordon, J. H. Jensen, S. Koseki, N. Matsunaga, K. A. Nguyen, S. J. Su, T. L. Windus, M. Dupuis, J. A. Montgomery, *J. Comput. Chem.* **14**, 1347 (1993).
- [25] <http://winmostar.com/jp/>
- [26] K. Tanaka, *J. Optoelectron. Adv. M.* **17**, 1716 (2015).
- [27] K. Tanaka, *J. Optoelectron. Adv. M.* **19**, 27 (2017).
- [28] R.A. Zingaro, W.C. Cooper, *Selenium* (Van Nostrand Reinhold, New York, 1974).
- [29] P. Andonov, *J. Non-Cryst. Solids* **47**, 297 (1982).
- [30] H. Wendel, *The Physics of Selenium and Tellurium* (eds.) E. Gerlach, P. Grosse (Springer 1979) 47-59.
- [31] J. Dresner, Stringfellow, *J. Phys. Chem. Solids* **29**, 303 (1968).
- [32] O.U. Vonwiller, *Nature* **104**, 347 (1919).
- [33] H. Koseki, A. Odajima, *Jpn. J. Appl. Phys.* **21**, 424 (1982).
- [34] H. Asao, K. Tanaka, *J. Appl. Phys.* **102**, 043508 (2007).
- [35] A. von Hippel, *J. Chem. Phys.* **16**, 372 (1948).
- [36] D. Emin, C.H. Seager, *Phys. Rev. Lett.* **28**, 813 (1972).
- [37] A.V. Kolobov, *J. Non-Cryst. Solids* **198-200**, 728 (1996).
- [38] A. Darbandi, O. Rubel, *Can. J. Phys.* **91**, 483 (2013).
- [39] M. Hiravama, R. Okugawa, S. Murakami, T. Mivake, *Phys. Rev. Lett.* **114**, 206401 (2015).
- [40] Y. A. Firsov, *Polarons in Advanced Materials*, ed. A.S. Alexandra (Springer 2007) p. 63.
- [41] F. K. Dolezalek, W.E. Spear, *J. Non-Cryst. Solids* **4**, 97 (1970).
- [42] K. Tanaka, *Phys. Stat. Sol. RRL* **00**, 1700254 (2017).
- [43] H. Lundt, G. Weiser, *Philos. Mag. B* **51**, 367 (1985).
- [44] R. Clement, J. C. Carballes, B. de Cremoux, *J. Non-Cryst. Solids* **15**, 505 (1974).